Impacts of Atmospheric Processes on ENSO Asymmetry: A Comparison between CESM1 and CCSM4

TAO ZHANG

Cooperative Institute for Research in Environmental Sciences, University of Colorado Boulder, and Physical Sciences Division, NOAA/Earth Systems Research Laboratory, Boulder, Colorado

XIAOLU SHAO

Nansen-Zhu International Research Centre, and Climate Change Research Center, Institute of Atmospheric Physics, Chinese Academy of Sciences, and University of Chinese Academy of Sciences, Beijing, China

SHUANGLIN LI

Nansen-Zhu International Research Centre, and Climate Change Research Center, Institute of Atmospheric Physics, Chinese Academy of Sciences, Beijing, and Department of Atmospheric Science, School of Environmental Studies, China University of Geosciences, Wuhan, China

(Manuscript received 26 May 2017, in final form 15 August 2017)

ABSTRACT

An evaluation of El Niño–La Niña asymmetry is conducted in the two recent NCAR coupled models (CCSM4 and CESM1) sharing the same ocean component. Results show that two coupled models generally underestimate observed ENSO asymmetry, mainly owing to an overestimate of the cold SST anomaly during the La Niña phase. The weaker ENSO asymmetry corresponds to a cold bias in mean SST climatology that is more severe in CESM1 than in CCSM4, despite a better performance in simulating ENSO asymmetry in the former. Corresponding AMIP (CAM4 and CAM5) runs are examined to probe the origin of the weaker ENSO asymmetry in coupled models. The analysis reveals a stronger time mean zonal wind in AMIP models, favoring a cold bias in mean SST. The bias of the stronger mean wind, associated with changes in mean precipitation, is more significant in CAM5 than in CAM4. The simulated skewness of the interannual variability of zonal winds is weaker than observations but somewhat improved in CAM5 compared to CAM4, primarily resulting from a more westward shift of easterly wind anomalies tied to the displacement of precipitation anomalies during the cold phase. Wind-forced ocean GCM experiments confirm that the bias in AMIP model winds can weaken ENSO asymmetry, with the contribution from the wind interannual variability being larger than from the mean winds. This demonstrates that the bias in ENSO asymmetry in coupled models can be traced back to the bias in the stand-alone atmosphere models to a large extent. The results pinpoint a pathway to reduce the bias in ENSO asymmetry in coupled models.

1. Introduction

A fundamental attribute of tropical Pacific variability is the asymmetry in equatorial SST anomalies between two extreme phases of El Niño–Southern Oscillation (ENSO). ENSO asymmetry results from the fact that the SST anomalies between the two extreme phases of ENSO are not mirror images of each other. This includes the observational evidence that the magnitude of SST anomalies over the eastern equatorial Pacific is larger during the ENSO warm phase compared to the cold phase and that there are spatial shifts in their respective patterns, causing a nonzero residual effect (Burgers and Stephenson 1999). Such an ENSO asymmetry has implications for U.S. seasonal forecasting for which ENSO is the primary skill source (Hoerling et al. 1997; Zhang et al. 2011, 2014, 2016). Also, given ENSO's global impact (Ropelewski and Halpert 1987; Kiladis and Diaz 1989; Hoerling et al. 1997; Wallace et al. 1998; Larkin and Harrison 2005; Zhang et al. 2011, 2016), understanding the cause and ensuring accurate simulation of ENSO asymmetry in climate models is important for reliable projections of climate change.

Corresponding author: Dr. Tao Zhang, tao.zhang@noaa.gov

DOI: 10.1175/JCLI-D-17-0360.1

Causes for the asymmetry on ENSO-related tropical Pacific SST variability are not clearly understood, but previous studies suggested that it is likely attributed to the nonlinear atmospheric or oceanic processes. Kang and Kug (2002) suggested that the relatively weak SST anomalies during La Niña compared to those during El Niño are associated with a westward shift of zonal wind stress anomalies, which is in turn due to the nonlinear dependence of deep convection on the tropical Pacific SST (Hoerling et al. 1997). An asymmetric wind response to SST forcing is also argued to be responsible for the ENSO asymmetry in later studies (Philip and van Oldenborgh 2009; Frauen and Dommenget 2010; Choi et al. 2013). In addition, some oceanic mechanisms have also been proposed to account for such an asymmetry. Vialard et al. (2001) argued that the cause for the ENSO asymmetry is the asymmetric negative feedback owing to tropical instability waves over the eastern Pacific, which have a relatively stronger effect during La Niña than during El Niño. Heat budget analysis of the ocean surface layer suggests that the nonlinear vertical temperature advection is a major contributor (Jin et al. 2003; An and Jin 2004). The analysis of updated ocean assimilation products reveals the key role of the nonlinear zonal and meridional ocean temperature advections but an opposite effect by the nonlinear vertical advection (Su et al. 2010). Based on the Bjerknes stability index (a measure of ENSO growth rate) analysis, a recent study by Im et al. (2015) found that the growth rate of El Niño events is larger than that of La Niña events and that an increased positive dynamical feedback during El Niño relative to La Niña is the major factor responsible for the ENSO amplitude asymmetry.

The residual effect due to the ENSO asymmetry, an indication of a nonzero forcing of the ENSO cycle, can be rectified into the mean state (Yeh and Kirtman 2004; Schopf and Burgman 2006; Sun and Zhang 2006; Sun et al. 2014) and therefore is fundamentally important to understand the decadal variability in the tropical Pacific (Rodgers et al. 2004; Sun and Yu 2009; Choi et al. 2009). The asymmetry in U.S. climate impacts, originating from teleconnections driven by ENSO extremes, reveals a rectified effect comprising a warmer eastern North America than would prevail in a climate lacking extreme ENSO variability (Zhang et al. 2016). The intensity of El Niño is found to affect California precipitation (e.g., Hoell et al. 2016). However, the incapacity of simulating ENSO asymmetry in many coupled models is mostly caused by the underestimate of the magnitude of El Niño events (Zhang and Sun 2014). To provide more realistic simulations of the extratropical climate, climate models need to accurately simulate the ENSO asymmetry.

Recognizing the key role of the asymmetric characteristics of ENSO in the tropical and extratropical climate, many researchers have extensively evaluated the performance of coupled climate models in simulating ENSO asymmetry over the past decades and found that the underestimate of the observed ENSO asymmetry is a prevalent problem (Burgers and Stephenson 1999; Hannachi et al. 2003; An et al. 2005; van Oldenborgh et al. 2005; Sun et al. 2013, 2016). However, those studies do not address the relationship of this bias in ENSO with other features of the climate in component models, through which we can isolate the sources of biases in climate models and better understand the cause for the biases in ENSO asymmetry. Zhang et al. (2009) analyzed the coupled runs of five successive versions of the Community Climate System Model (CCSM) as well as their corresponding atmosphere-only (AMIP) runs and noted a dependence of the strength of the simulated ENSO asymmetry on the utilized convective scheme. Regardless of model generation, however, Zhang et al. (2009) found an underestimate in ENSO asymmetry in all studied NCAR coupled models. This continues to be a systematic bias occurring across many other modeling systems. In a recent study examining the multiple coupled models constituting CMIP5 (Taylor et al. 2012), Zhang and Sun (2014) evaluated 14 different models together with their corresponding AMIP runs and showed that an underestimate of the ENSO asymmetry is a common bias in these state-of-the-art climate models. With the aid of wind-forced ocean GCM experiments, they suggested that the weaker ENSO asymmetry originates partially from the atmospheric processes.

The findings of Zhang and Sun (2014) are based on the numerical experiments forced by a multimodel ensemble mean of AMIP winds. It is unclear whether these findings are a symptom of error cancelations in the multimodel mean or will also hold for individual models. In addition, it is hard to compare the effect of wind biases among models since CMIP5 coupled models have different ocean components as well. The contributions from different ocean components to ENSO asymmetry may not be the same because they may have a different oceanic response to the same wind stress. Therefore, the cause for the weakened ENSO asymmetry in climate models remains elusive, and a pathway for model improvement is not yet evident.

In the present study, we evaluate the ENSO asymmetry in the two latest CCSM models [Community Climate System Model, version 4 (CCSM4), and Community Earth System Model, version 1 (CESM1)] that have the same ocean component. We extend the study of Zhang and Sun (2014) to further address the impact of

atmospheric processes on ENSO asymmetry with the purpose of obtaining more insights into the possible cause for the bias in ENSO asymmetry. The results may help to point toward a pathway to reduce the bias in the simulation of ENSO asymmetry in coupled models. The observational and model datasets as well as the methodology of our analysis are described in section 2. Section 3 first presents the analysis of ENSO asymmetry in two coupled models and then the asymmetry in the corresponding AMIP runs. Last, forced ocean model experiments driven by individual AMIP winds are performed to understand the effect of bias in the atmospheric response on ENSO asymmetry. Conclusions and a discussion are given in section 4.

2. Data and methods

We evaluate the ENSO asymmetry in historical simulations of the two latest NCAR coupled models archived at CMIP5 datasets (Taylor et al. 2012), which include CCSM4 (Gent et al. 2011) and CESM1 (Hurrell et al. 2013). Both CESM1 and CCSM4 utilize the Los Alamos National Laboratory (LANL) Parallel Ocean Program, version 2 (POP2; Smith et al. 2010), as the ocean model component. The atmospheric component of CCSM4 is the Community Atmosphere Model, version 4 (CAM4; Neale et al. 2013), while that of CESM1 is the Community Atmospheric Model version 5 (CAM5; Neale et al. 2012). Both atmospheric components are run at ~1° horizontal resolution but at different vertical levels, with 26 levels in CAM4 and 30 levels in CAM5. Except for the Neale et al. (2008) deep convection scheme, CAM5 has been modified significantly with a range of enhancements and improvements in the parameterizations of physical processes since CAM4. These key changes include the new parameterizations of shallow convection, radiation, boundary layer, cloud microphysics, and aerosols (Neale et al. 2012; Hurrell et al. 2013; Meehl et al. 2013). A new shallow convection scheme (Park and Bretherton 2009), which uses a realistic plume dilution equation and closure that accurately simulates the spatial distribution of shallow convective activity, is incorporated in CAM5 to replace the Hack (1994) scheme in CAM4. The radiation scheme has been updated from the schemes of Collins (2001) and Collins et al. (2002) to the Rapid Radiative Transfer Method for GCMs (RRTMG) and employs an efficient and accurate correlated-k method for calculating radiative fluxes and heating rates (Iacono et al. 2008). In addition, CAM5 uses a new moist turbulence scheme (Bretherton and Park 2009) for the replacement of Holtslag and Boville (1993) scheme used in CAM4. Stratiform microphysical processes are represented by a prognostic, two-moment formulation for cloud droplet and cloud ice and liquid mass and number concentrations (Morrison and Gettelman 2008) in place of the single-moment (Rasch and Kristjansson 1998) scheme used in CAM4. The indirect aerosols effects are not included in CAM4, but they can be estimated with CAM5 using the new aerosol scheme (Liu et al. 2012).

To quantify the impact of changes in the parameterization schemes on the ENSO asymmetry, we diagnose the skewness of simulated SST anomalies in the two coupled models as in previous studies (Zhang et al. 2009; Zhang and Sun 2014). Also, composites of El Niño and La Niña are constructed to determine which ENSO phase contributes most to the ENSO asymmetry bias. Furthermore, we will apply an alternative approach to measure ENSO asymmetry based on the SST residual defined as the sum of the composite anomalies between two phases of ENSO. The comparison of these two approaches (skewness and residual) will reveal the robustness of the results. These approaches will also be applied to other model and observational variables including precipitation and surface zonal wind stress.

The observational data used for model evaluation are the same as those used by Zhang et al. (2009) and Zhang and Sun (2014). The SST data are from the Hadley Centre Sea Ice and SST dataset (HadISST; Rayner et al. 2003). The wind stress data are obtained from the Simple Ocean Data Assimilation (SODA) set (Carton and Giese 2008). Observations of precipitation are obtained from the Climate Prediction Center (CPC) Merged Analysis of Precipitation (CMAP; Xie and Arkin 1997).

In addition to examining the asymmetry in coupled models, we will also evaluate the corresponding AMIP simulations from CAM4 and CAM5 to determine whether the ENSO asymmetry biases can be traced back to the atmospheric origins—in particular the tropical winds. Subsequently, to verify the impact of atmospheric processes on ENSO asymmetry, the NCAR Pacific basin model (Gent and Cane 1989), which simulates well the observed characteristic of ENSO (Sun 2003; Sun et al. 2004; Sun and Zhang 2006; Sun et al. 2014; Zhang and Sun 2014), will be utilized to perform a suite of specifically designed ocean experiments driven by CAM4 and CAM5 AMIP wind fields, respectively.

3. Results

a. *Asymmetry in CCSM4 and CESM1 coupled runs*

A quantitative measure of the ENSO asymmetry reveals that in general the two NCAR models underestimate the observed ENSO asymmetry. Figure 1 shows the skewness of Niño-3 SST anomalies from

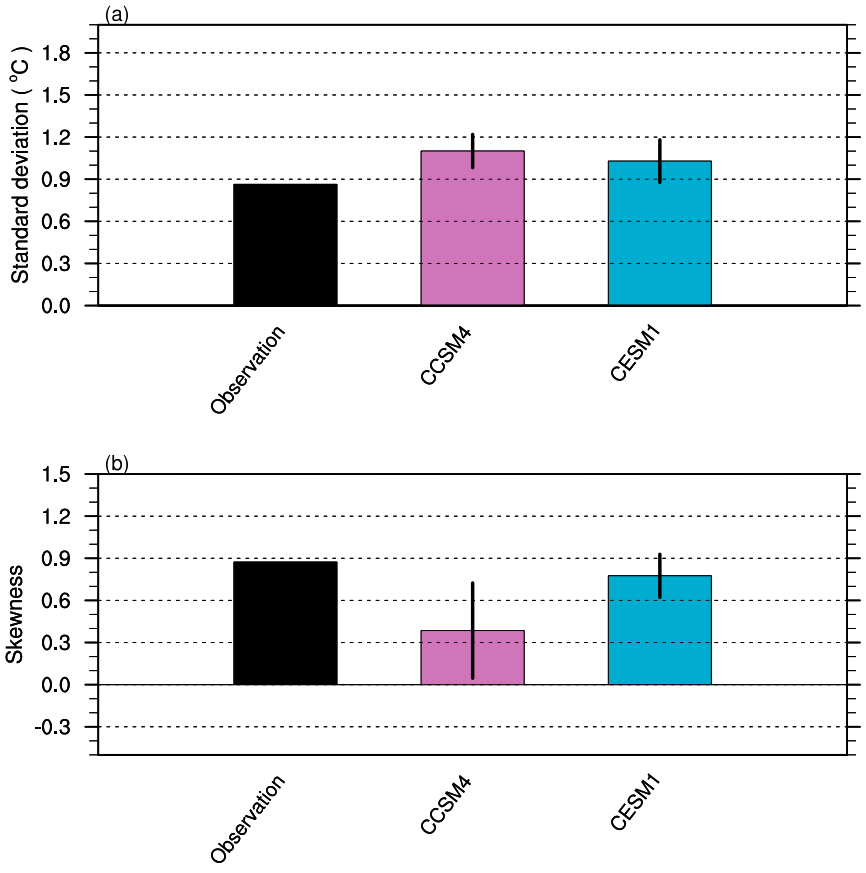

FIG. 1. The (a) standard deviation and (b) skewness of monthly Niño-3 SST anomalies from observations and coupled model simulations. The length of data for computing the standard deviation and skewness is 56 yr (1950–2005). The figure shows the mean of the samples and the standard deviation across the samples (eight members from CCSM4 and four members from CESM1 in CMIP5 datasets).

observations and the two models, together with their variance. Measured by the variance of Niño-3 SST, the simulated ENSO in the two NCAR models is as strong as in observations. In comparison, the variability of ENSO in CCSM4 is somewhat stronger while that in CESM1 is more comparable to observations. Measured by the skewness of Niño-3 SST, however, the two models simulate an overall weaker than observed positive ENSO asymmetry. By contrast, the bias of the underestimate of the Niño-3 SST skewness is more prominent in CCSM4 but somewhat improved in CESM1. The results support previous findings based on CMIP5 models that the stronger ENSO variability does not guarantee a stronger ENSO asymmetry (Zhang and Sun 2014).

The bias in ENSO asymmetry could be linked to the bias in mean SST state. Figure 2 indicates that the weak ENSO asymmetry in the two models corresponds to a cold bias in the mean SST climatology, which is a prevalent problem in coupled models (Sun et al. 2006; Zhang et al. 2009; Zhang and Sun 2014; Sun et al. 2016). Interestingly, despite an improvement in the simulation of ENSO asymmetry, the cold bias in mean SST state is more worrisome in CESM1 relative to CCSM4, as the former has a stronger (above 1°C) cold bias that extends far westward.

The skewness map of SST anomalies shows that there is a positive skewness over the eastern tropical Pacific in observations, indicating that the observed SST anomalies in the eastern Pacific are skewed toward warm events (Fig. 3a). The two coupled models simulate the pattern of observed positive SST asymmetry over the eastern Pacific (210°–270°E, 10°S–10°N), where the pattern correlation with observations is about 0.65 in CCSM4 and 0.70 in CESM1, respectively (Figs. 3b,c). However, the magnitude is somewhat underestimated especially in CCSM4, consistent with the skewness results shown in Fig. 1. We also note that the stronger SST skewness in CESM1 extends too far westward, along with a wider meridional extension than in CCSM4. To

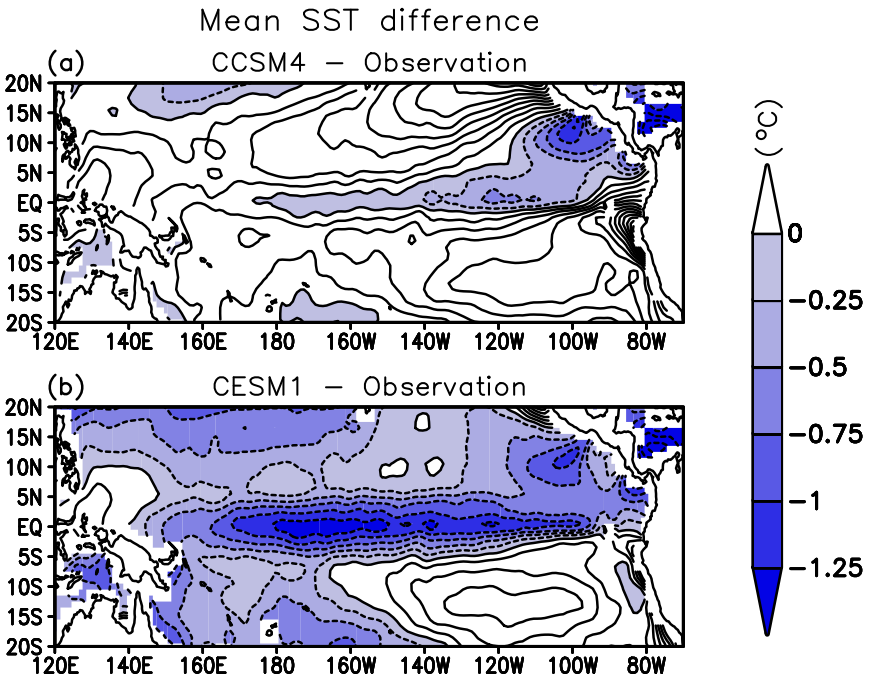

FIG. 2. (a) The difference between observations and ensemble mean SST annual climatology from CCSM4 and (b) the difference between observations and ensemble mean SST annual climatology from CESM1. The length of data for computing is 56 yr (1950–2005).

examine the robustness of the results, we have constructed the composites of warm events and cold events and used the sum of the SST anomalies between two phases of ENSO as SST residual effect to get an alternative measure of ENSO asymmetry (Figs. 3d–f). The SST residual results are found to be similar to the SST skewness map, although the former is based on linear calculation and the latter is based on nonlinear calculation (Burgers and Stephenson 1999; Hannachi et al. 2003; An et al. 2005; van Oldenborgh et al. 2005; Zhang et al. 2009; Zhang and Sun 2014; Sun et al. 2013, 2016). This confirms the impression that in general the two NCAR models underestimate the observed positive ENSO asymmetry over the eastern tropical Pacific. The slight improvement in the simulation of ENSO asymmetry in CESM1 relative to CCSM4 is mostly due to a wider meridional extension and a far-westward shift. To better understand the cause for the underestimate of the skewness in the two coupled models, the probability distribution function (PDF) pattern of Niño-3 SST anomalies from observations and coupled models is displayed (Fig. 3g). The observed maximum positive anomalies can reach about 3.5°C, but the maximum negative anomalies are about −2°C, in agreement with the observed positive skewness (Fig. 1). The two models can capture the observed maximum positive anomalies and even have somewhat larger probability of the occurrence for a band of warm anomalies ranging from 0.5° to 3.5°C. The magnitude of the maximum cold event anomalies is overestimated in the two models (about 1°C colder than observations). It can also be seen that the probability of strong cold anomalies (from −3° to −1.25°C) in CCSM4 is higher than that in CESM1. The results indicate that the overestimate of the cold anomalies is the major cause for the weaker ENSO asymmetry in the two coupled models.

To further explore whether the cold phase of ENSO contributes most to the bias of ENSO asymmetry, we investigate the spatial distribution of composite anomalies during two phases of ENSO (Fig. 4). In observations, the positive SST anomalies associated with warm events extend farther to the South American coast and have a relatively larger magnitude compared to the negative SST anomalies associated with cold events, resulting in a stronger ENSO asymmetry over the eastern Pacific as noted earlier (Fig. 3). The observed maximum warming center around 110°W during El Niño events is well captured in the two models, but the underestimate of the warm SST anomaly in the coastal regions (100°–80°W) is evident in CESM1. The observed negative SST anomaly during La Niña events is somewhat overestimated (about 0.2°~0.4°C) in the models, especially in CCSM4. Therefore, our analysis further supports the argument that the overestimate of the

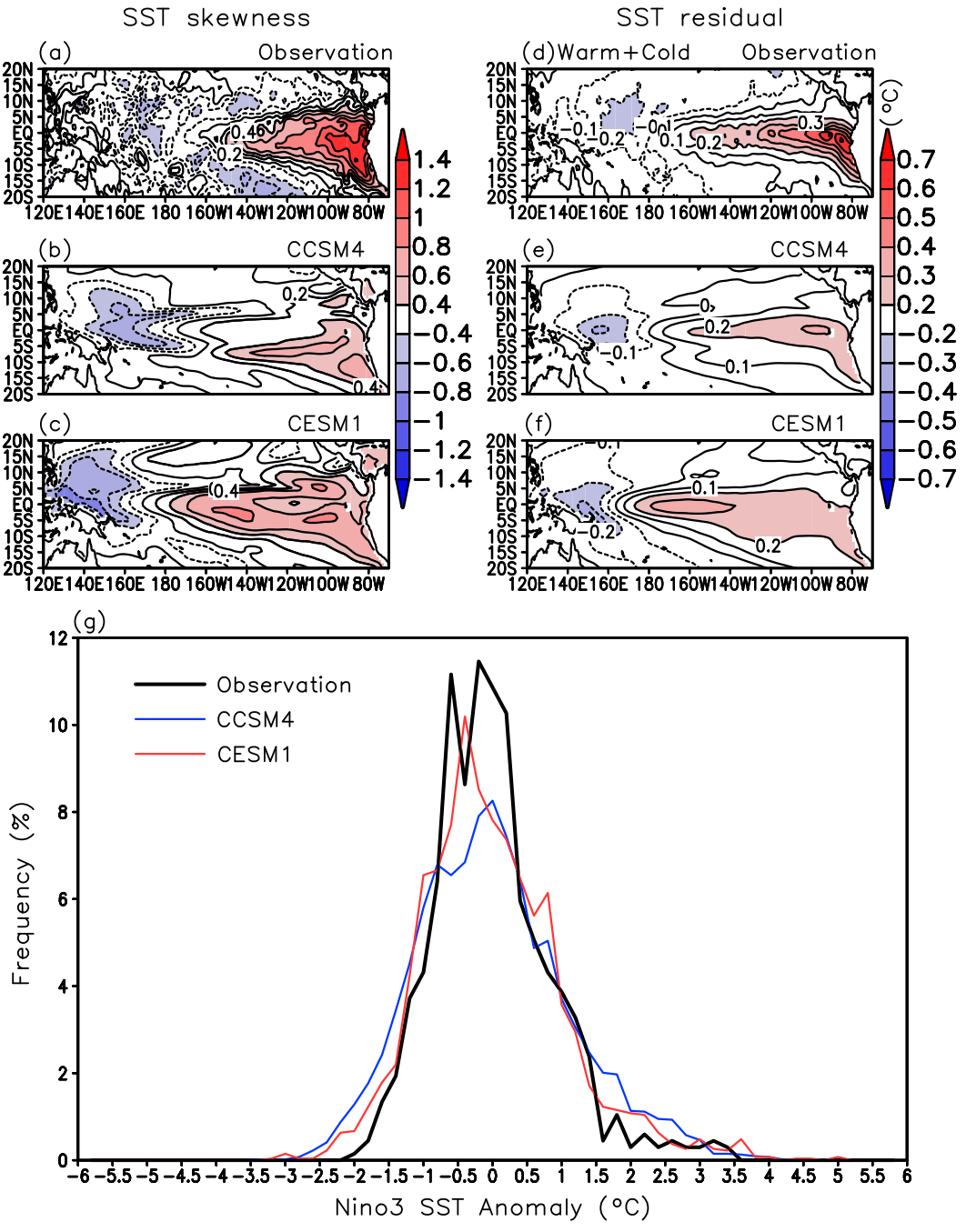

FIG. 3. (a)–(c) The skewness pattern of SST anomalies, (d)–(f) the residual of composite SST anomalies between two phases of ENSO, and (g) PDF of Niño-3 SST anomalies from observations and coupled models. The positive (negative) anomalies of Niño-3 SST with the magnitude greater than 0.5°C are selected to construct composites of warm (cold) events following the method of Zhang and Sun (2014). The length of data for computing is 56 yr (1950–2005).

observed negative SST anomaly during the cold phase of ENSO is the major contributor to the weak ENSO asymmetry in the NCAR models, in agreement with the previous PDF results. The relatively larger ENSO asymmetry in CESM1 than in CCSM4 is also mainly due to the improvement of the simulation during the cold phase (see also Fig. 3g). This is because the Niño-3 SST warm anomaly in CCSM4 is even slightly stronger (about 0.07°C) than in CESM1, which would imply a greater ENSO asymmetry in the former. However, the

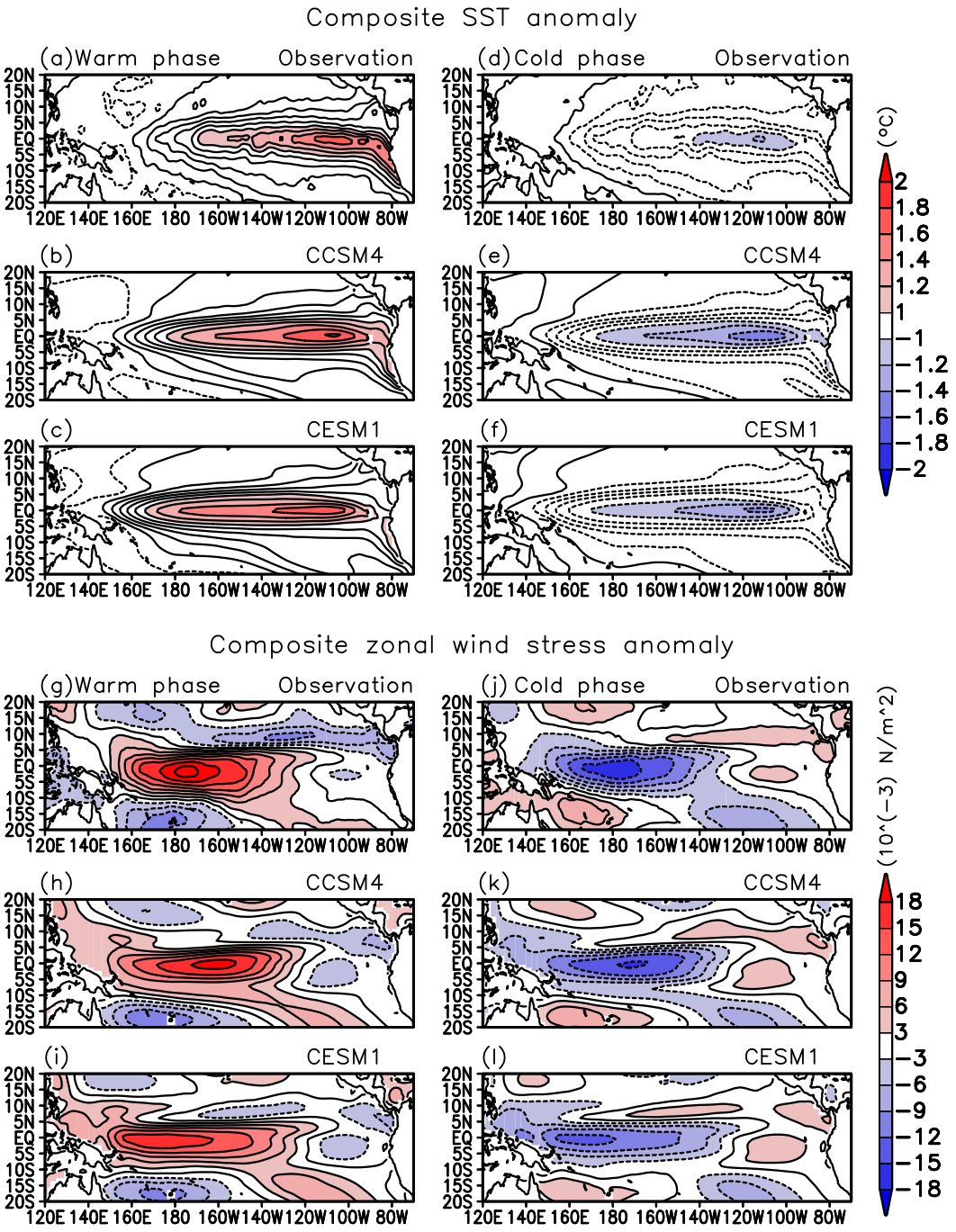

FIG. 4. The spatial distributions of composite SST anomalies from observations and coupled models during (a)–(c) the warm phase and (d)–(f) cold phase of ENSO. (g)–(l) Corresponding anomalies for zonal wind stress. The length of data used in the calculation is 56 years for all the models and observed SST (1950–2005) and 50 years for SODA zonal wind stress (1959–2008).

bias in the Niño-3 SST cold anomaly in CCSM4 is somewhat larger (about 0.10°C) than in CESM1. Therefore, the relatively larger (about 50%) difference in SST anomaly between the two models during the cold phase compared to the warm phase is likely the major factor responsible for the weaker ENSO asymmetry in CCSM4 relative to CESM1. A systematic bias is found in the two coupled models that have strong warm and cold anomalies extending too far to the west in contrast to observations during two phases of ENSO. This

westward extension bias is also noted in the mean SST state of the two models that have an excessive cold tongue (Fig. 2).

The pattern of SST anomalies during two phases of ENSO is closely tied to the pattern of surface wind stress anomalies. In line with the magnitude asymmetry of ENSO in reality, observations show a relatively larger maximum westerly wind stress anomaly during El Niño events than the corresponding easterly wind stress anomaly during La Niña events in the central Pacific (Figs. 4g,j). Furthermore, the observed center of the equatorial zonal wind stress shows a westward shift during the cold phase relative to the warm phase, locating at about 170°W during the warm phase and at 180° during the cold phase. Despite the incapability in capturing the location of observed maximum centers, the two coupled models reproduce well the magnitude asymmetry of zonal wind stress anomalies between two phases of ENSO (Figs. 4h,i,k,l). Accompanied with the westward extension of SST anomalies during two phases of ENSO, zonal wind stress anomalies in the two models also extend to the far-western Pacific having a larger magnitude than observations. Assuming a similar sensitivity of the ocean to surface wind anomalies between models and observations, the overly strong zonal wind stress anomalies in the western Pacific may result in an enhanced zonal current and thus produce an efficient zonal temperature advective feedback that causes an excessive warming (cooling) in the west-central Pacific during El Niño (La Niña) events. Based on CMIP5 multimodel-mean results, Taschetto et al. (2014) found a similar linkage between the bias in zonal wind stress anomalies over the western Pacific and the bias in SST anomalies during two phases of ENSO. We also note that during the cold phase CESM1 has the relatively weaker and more westward-displaced easterly wind anomalies compared to CCSM4, which is likely responsible for the relatively weaker negative SST anomalies in the former. The results suggest that the intensity and location of wind stress anomaly may be key factors for improving the asymmetry between El Niño and La Niña events.

b. *Asymmetry in CAM4 and CAM5 AMIP runs*

The above analysis links the bias in SST field to the bias in zonal wind stress field in coupled models. However, the cause for the bias in the complex coupled system is difficult to identify because of the strong feedbacks of the tropical Pacific ocean–atmosphere system. Is the bias in the SST field a consequence of the bias in zonal wind stress field or the cause of the latter? To answer this question, and more generally to explore the causes of ENSO asymmetry, we conduct the composite analysis from the corresponding AMIP runs of CCSM4 and CESM1 that are forced with the observed SST boundary conditions and attempt to explore whether the bias in coupled models can be traced back to the bias in the stand-alone atmosphere models.

We have calculated the spatial pattern of skewness of interannual zonal wind stress anomaly from observations and AMIP runs of the two models (Fig. 5). The AMIP runs involve subjecting the atmospheric component of the two coupled models to the observed SST variability and thus having identical ENSO asymmetry to that in observations. Results show that in observations, there is a broad positive skewness of zonal wind stress over the tropical Pacific with the maximum center locating in the central Pacific (Fig. 5a). Although the SSTs now are the same as those observed, the skewness of zonal wind stress is notably weaker in the two AMIP models (Figs. 5b,c). In contrast to CAM4, CAM5 increases the simulated zonal wind stress skewness across the equatorial Pacific, where the improvement of central Pacific wind stress skewness is evident (Fig. 5d). This may explain in part why the above-mentioned coupled models generally have a weaker ENSO asymmetry and CESM1 has a relatively larger SST skewness compared to CCSM4 (Fig. 1).

To understand the difference in the skewness map of zonal wind stress between AMIP runs and observations, we examine their spatial distributions of composite anomalies of zonal wind stress and precipitation during two phases of ENSO (Fig. 6). Both models capture the observed maximum magnitude of zonal wind stress over the central Pacific during El Niño and La Niña events (Figs. 6a–f). However, unlike observations that have an approximately 10° shift between two phases of ENSO, the simulated maximum centers seem to be locked at the location of about 170°W in the models. The lack of the shift of the maximum wind stress centers between two phases of ENSO may be responsible for the weaker skewness of zonal wind stress in the models. A close examination of zonal wind stress anomaly over the western Pacific reveals that CAM5 has a more westward shift of easterly wind anomaly compared to CAM4 (indicated by green lines shown in Figs. 6e,f) during the cold phase, favoring an increase in the skewness of zonal wind stress. Such a shift is also evident in the corresponding coupled models (Figs. 4k,l).

The asymmetric response of zonal wind stress to ENSO is linked to the nonlinear dependence of the deep convection on SST (Kang and Kug 2002; Zhang et al. 2009). We have examined the composite precipitation anomalies from observations and AMIP runs during two phases of ENSO (Figs. 6g–l). Aligned with the displacement of zonal wind stress, the observed

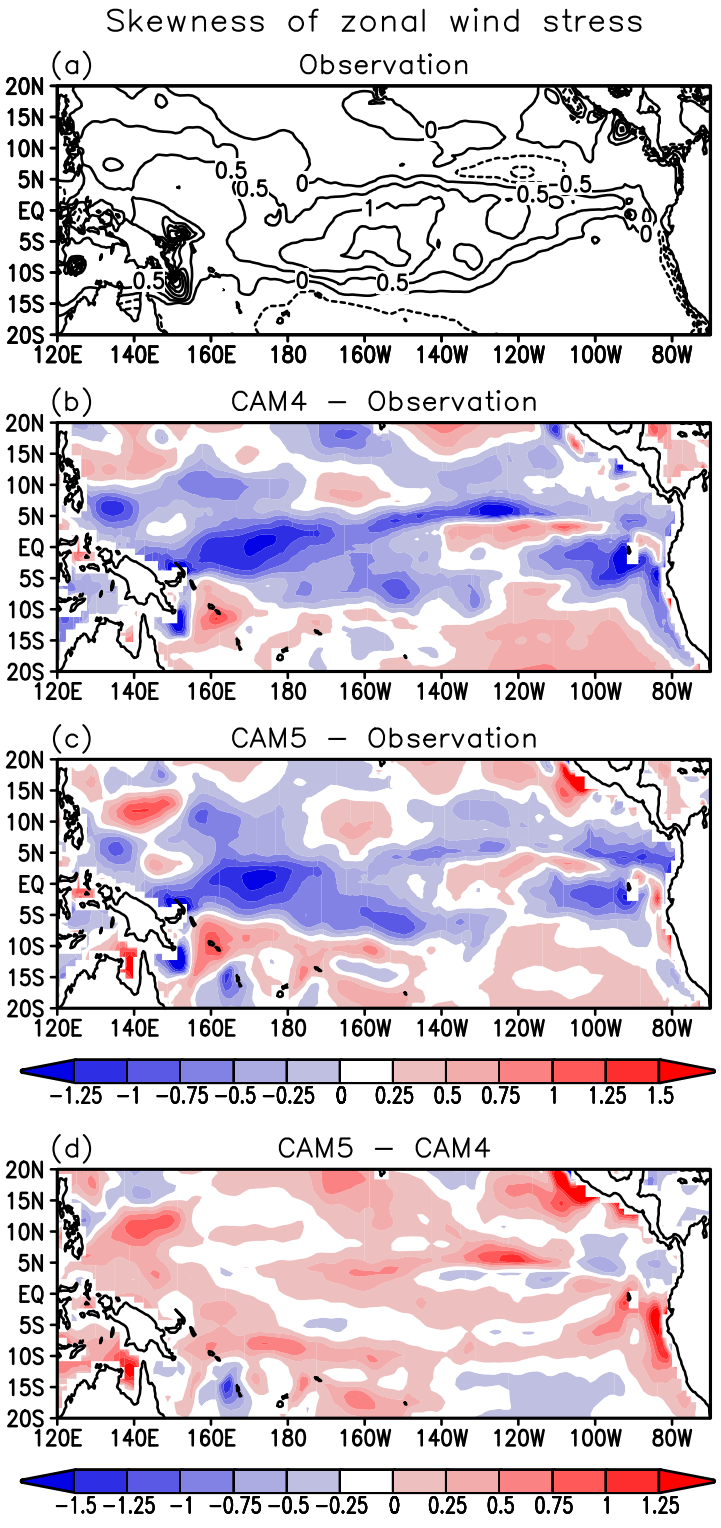

FIG. 5. The spatial pattern of skewness of zonal wind stress from (a) observations, (b) the difference between CCSM4 AMIP run (CAM4) and observations, (c) the difference between CESM1 AMIP run (CAM5) and observations, and (d) the difference between CESM1 AMIP run and CCSM4 AMIP run. The analysis is computed over the period of 1979–2005 based on six-member ensemble mean from CCSM4 AMIP runs and two-member ensemble mean from CESM1 AMIP runs in CMIP5 datasets.

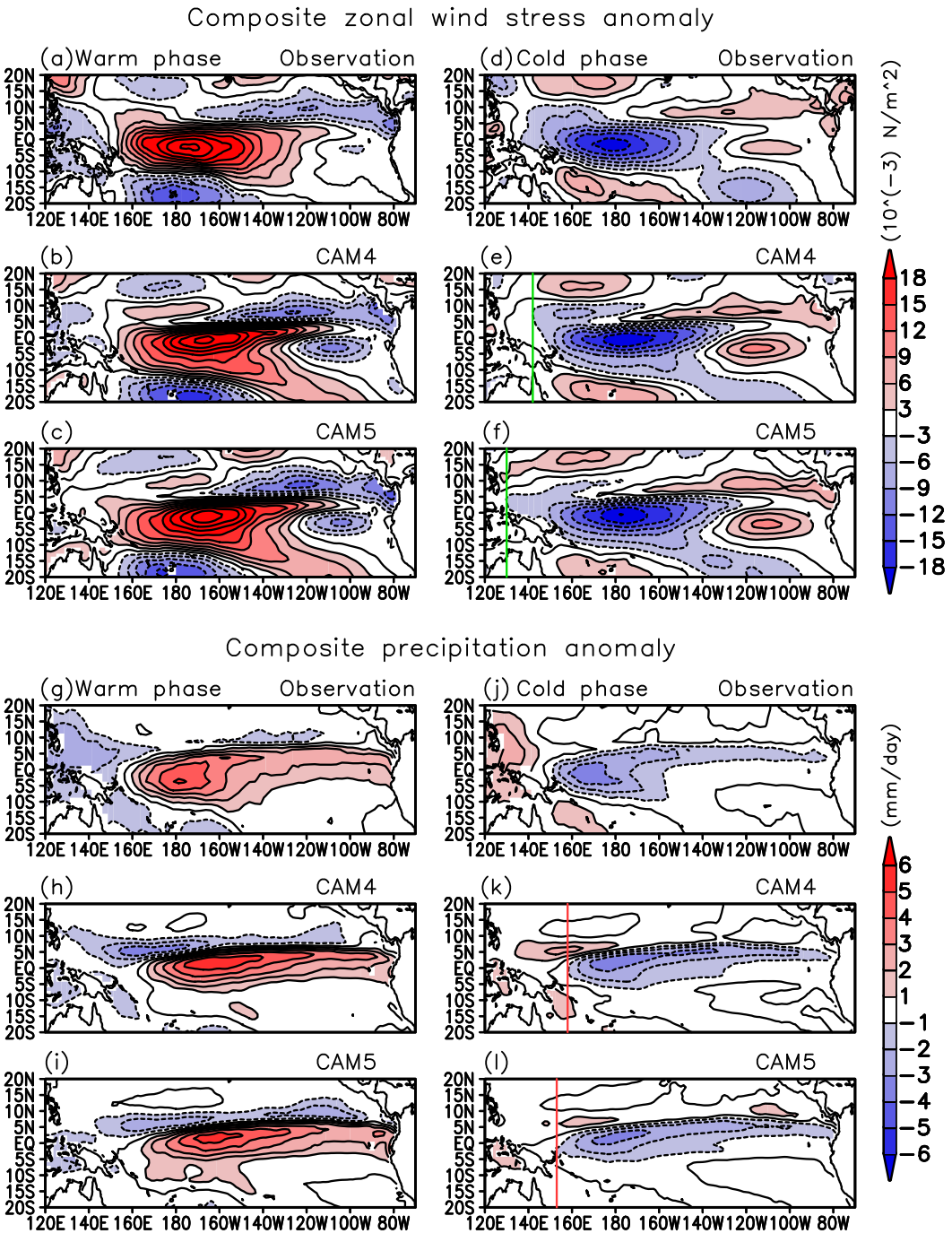

FIG. 6. The spatial distributions of composite zonal wind stress anomalies from observations and AMIP models during (a)–(c) the warm phase and (d)–(f) cold phase of ENSO. (g)–(l) Corresponding anomalies for precipitation. Green and red lines indicate the positions that the equatorial easterly wind anomalies and negative precipitation anomalies can reach, respectively. The length of data used in the calculation is 27 years (1979–2005).

precipitation anomaly shows an obvious spatial shift between two phases of ENSO. Similar to the difference in zonal wind stress, the negative precipitation anomaly during the cold phase in CAM5 extends westward by about 5° relative to CAM4 (indicated by red lines shown in Figs. 6k,l). In contrast to observations, the positive precipitation anomalies over the central Pacific during the warm phase tend to shift eastward and northward in the two models. A similar feature is also visible in the zonal wind stress during the warm phase.

In addition to the bias in the variability of zonal wind stress, AMIP models also have biases in the time-mean states. Figure 7 shows that CAM4 has stronger mean winds than observations over most regions of the equatorial Pacific, especially over the equatorial eastern Pacific (Fig. 7a). The bias of stronger mean winds is more severe in CAM5, which also has a stronger equatorial mean wind than CAM4 (Figs. 7b,c). This may contribute to the cold bias of mean SST states in the two coupled models and the relatively larger bias in CESM1 (Fig. 2). The effect of bias in mean winds on the bias in mean SST state will be further examined by conducting numerical experiments in the following subsection.

The stronger mean winds in CAM5 with respect to CAM4 are linked to the difference in mean precipitation between the two models, which is characterized with generally more precipitation over the warm pool region and less precipitation over the eastern Pacific in the former (Fig. 7d). Therefore, there is an east–west asymmetry in the mean precipitation difference between the two models, and the resulting excessive zonal latent heating gradient associated with zonal precipitation gradient may drive the stronger mean winds in CAM5 (Lin 2007).

To further examine the evidence for the linkage between the difference in mean precipitation and the difference in mean zonal winds, we have utilized a linear baroclinic model (LBM) (Peng and Whitaker 1999) to perform numerical experiments. The LBM is driven by an idealized tropical heating anomaly pattern similar to the mean precipitation difference between the two models and imposed on a climatological annual basic state, in order to address the possible cause of climatological wind differences that could result from mean precipitation changes. The response of the LBM to the forcing of tropical heating anomaly is similar to the difference in mean zonal wind stress between the two models over most regions of the equatorial Pacific, where a broad easterly wind is dominant (Fig. 7f vs Fig. 7c). This supports the argument that changes in mean precipitation from CAM4 to CAM5 may contribute to the deterioration of mean equatorial zonal winds in CAM5.

c. *Wind-forced ocean GCM experiments*

To examine the effect of biases of mean model winds associated with convection in AMIP runs on the tropical SST mean state, we use individual model mean winds to drive the NCAR Pacific basin model (Sun and Zhang 2006; Zhang and Sun 2014) and perform the spinup runs without ENSO for a short-term integration. The results are compared with the similar runs but forced by observed mean winds (Fig. 8). These short-term experiments will be used to understand whether the model climatological winds trigger an initial cold bias in mean SST, which helps to isolate the time scales of bias development and the responsible processes. Numerical experiments indicate that the model mean winds tend to cause a colder mean SST state. The CAM5 model winds trigger a much colder mean SST state, and this cold bias can be further amplified in coupled models as seen in Fig. 2.

We have also utilized the NCAR Pacific basin model to carry out the parallel runs with ENSO to explore the relative importance of biases in mean wind stress and biases in the variability of interannual wind from the two AMIP runs to the simulation of ENSO asymmetry. By expanding the experiment design of Zhang and Sun (2014) to the individual AMIP models (Table 1), the present numerical experiments provide a better understanding of the effect of atmospheric processes on ENSO asymmetry in the two coupled models that share the same ocean component. First, as a baseline, a forced ocean experiment will be run in which both climatological winds and interannual variability of winds are the same as those from observations (experiment 1). To understand the effect of biases in mean winds, we then replace the observed climatological winds with CAM4 and CAM5 climatological winds, respectively, but keep the observed interannual anomalies of winds unchanged in the experiments (experiments 2a and 2b). Subsequently, to further examine the role of modeled interannual anomalies of winds on ENSO asymmetry, we use the actual model winds from CAM4 and CAM5 that include the simulated climatology and interannual anomalies to drive the ocean (experiments 3a and 3b). Finally, to investigate the role of observed climatological winds, we replace the CAM4 and CAM5 climatological winds with the observed counterpart but keep the interannual anomalies of model winds unchanged in the experiments (experiments 4a and 4b).

Table 1 shows the standard deviation and skewness of the interannual variability in Niño-3 SST from seven forced ocean runs with the NCAR Pacific basin model. We have tested the model for its suitability and found that when driven by observed winds (experiment 1) the NCAR Pacific basin model realistically reproduces the observed skewness of Niño-3 SST anomalies (see also Zhang and Sun 2014). Compared to the skewness value in the run by observed winds (1.20 in experiment 1), the skewness in the runs forced by full model winds from CAM4 (0.57 in experiment 3a) and CAM5 (0.79 in experiment 3b) is underestimated by about 53% and 34%, respectively, together with a reduced variability. We also note that there is a relatively larger skewness in the run forced by CAM5 full winds than by CAM4 full

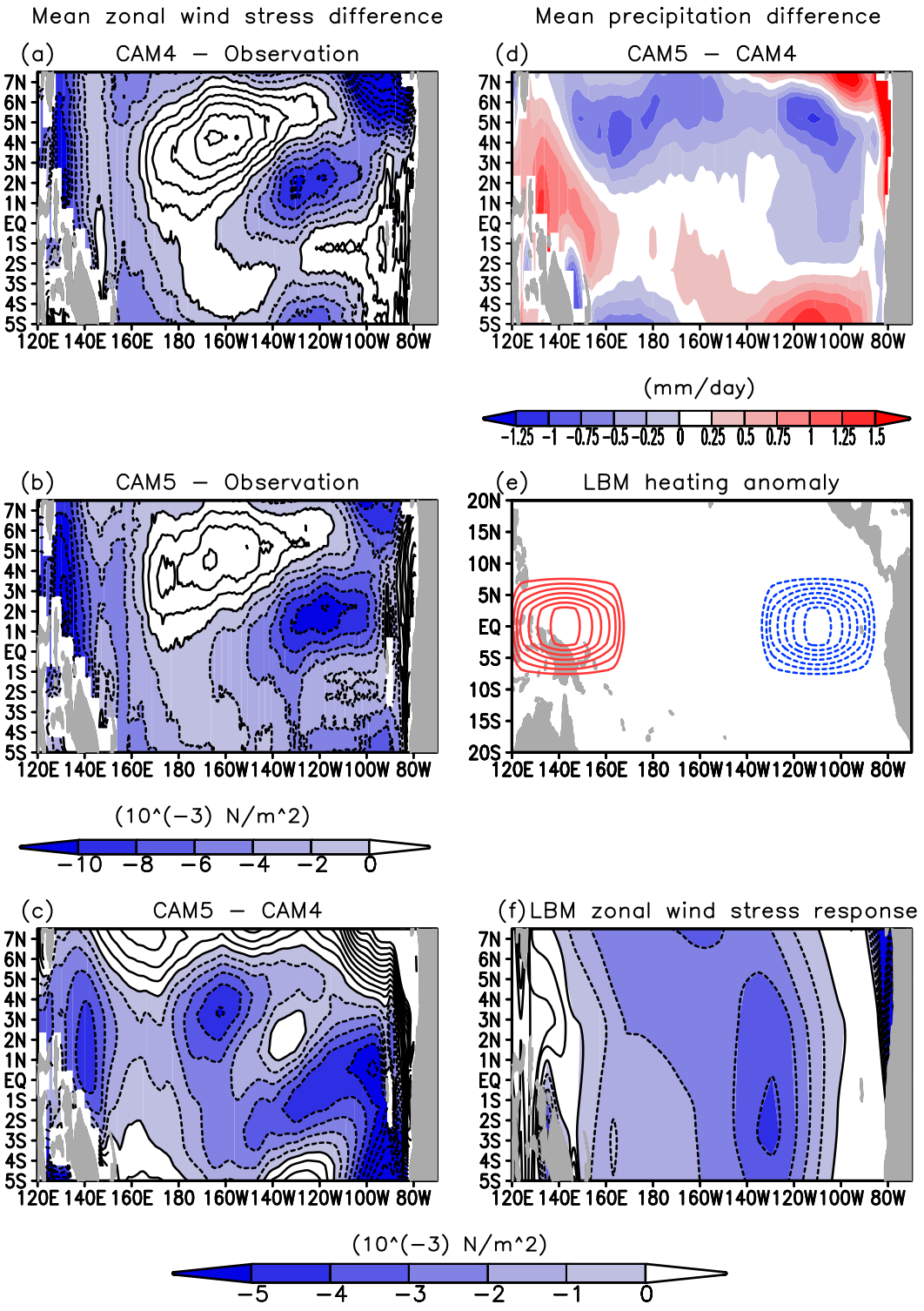

FIG. 7. The difference in zonal wind stress annual climatology (a) between CCSM4 AMIP runs and observations, (b) between CESM1 AMIP runs and observations, and (c) between CESM1 AMIP runs and CCSM4 AMIP runs. (d) The difference in precipitation annual climatology between CESM1 AMIP runs and CCSM4 AMIP runs. (e) Idealized diabatic heating pattern used to force the LBM, which is similar to the mean precipitation difference between the two models. (f) LBM simulated zonal wind stress response to the forcing of anomalous diabatic heating. The specified heating anomalies have maximum values of 1 K day^{-1} at 350 hPa. Shown are LBM results based on the average of the last 5 days of a 50-day integration in order to obtain the steady solution.

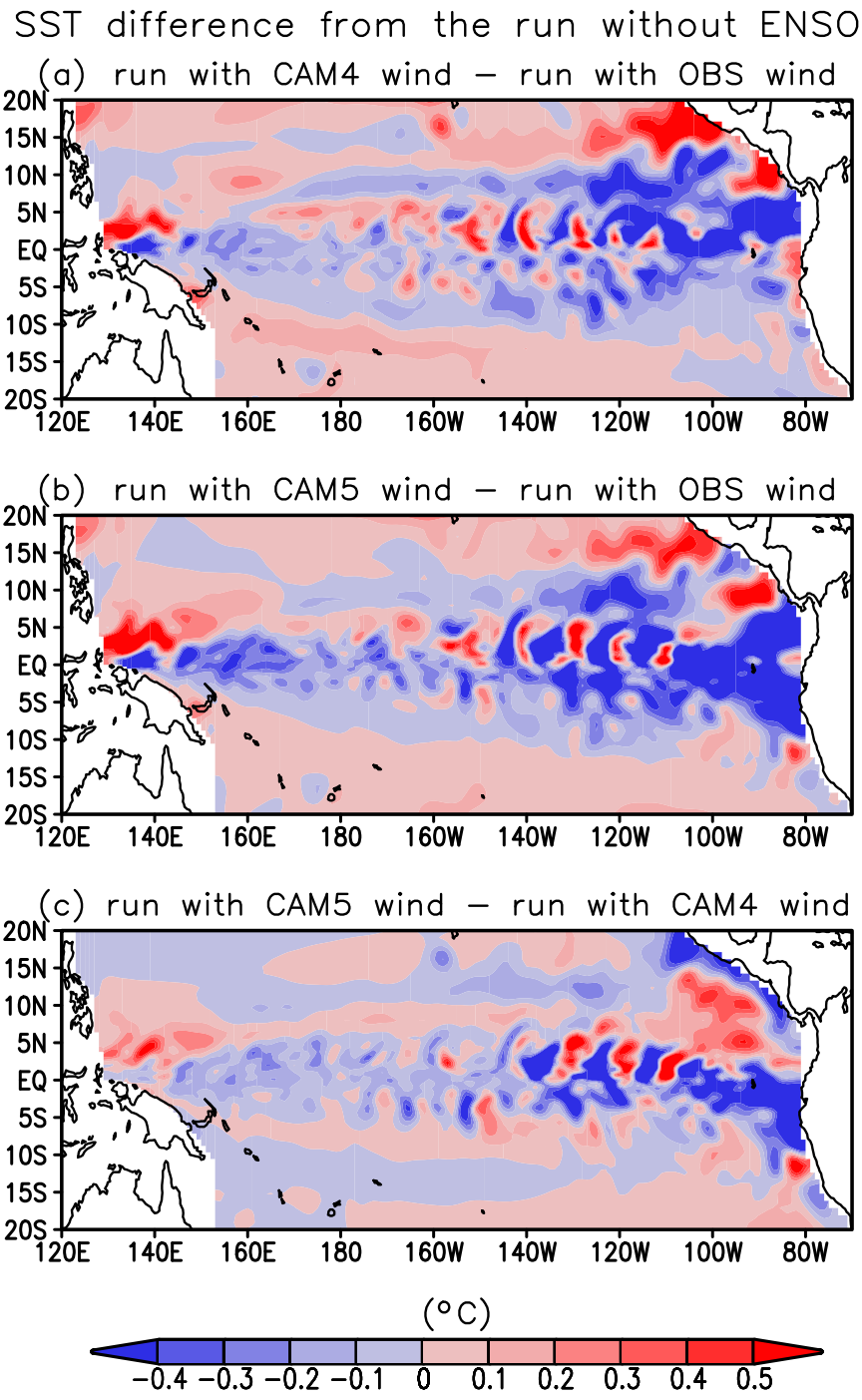

FIG. 8. The mean SST difference in the run without ENSO forced by climatology winds. SST difference (a) between the run forced by observed winds and the run by CCSM4 AMIP winds, (b) between the run forced by observed winds and the run by CESM1 AMIP winds, and (c) between the run forced by CCSM4 AMIP winds and the run by CESM1 AMIP winds. Shown are the results based on 3-month-long integrations, in order to understand whether the bias in mean surface winds can initiate the bias in mean SST.

TABLE 1. Standard deviation and skewness of the interannual variability in Niño-3 SST from seven forced ocean model experiments. The mean as well as the anomaly part of the surface winds used in these experiments are listed. The length of wind data used in the forced runs is 27 yr for both SODA wind stress and AMIP runs (1979–2005).

Experiment ID (label in figures)	Surface wind stress		Statistics of Niño-3 SSTA	
	Climatology	Anomaly	Skewness	Standard deviation (°C)
Experiment 1	Observation	Observation	1.20	0.83
Experiment 2a	CCSM4 AMIP	Observation	1.10	0.80
Experiment 2b	CESM1 AMIP	Observation	1.06	0.75
Experiment 3a	CCSM4 AMIP	CCSM4 AMIP	0.57	0.68
Experiment 3b	CESM1 AMIP	CESM1 AMIP	0.79	0.65
Experiment 4a	Observation	CCSM4 AMIP	0.73	0.73
Experiment 4b	Observation	CESM1 AMIP	1.09	0.74

winds, consistent with what we have found in the two coupled models (Fig. 1). The results demonstrate that the bias in coupled systems can be revealed in the bias inherent in the stand-alone atmosphere models. The comparison between the runs using the same observed wind anomaly but different wind climatology (experiments 1, 2a, and 2b) shows that the bias in the CAM4 (CAM5) wind climatology contributes to about 15% (30%) of the reduction in ENSO asymmetry, implying a dominant role of the bias in simulated wind interannual anomalies. Note that the contribution from the bias in CAM4 wind climatology to the reduction in ENSO asymmetry is relatively small compared to that from the bias in CAM5 wind climatology. This is expected because the bias in the mean winds in CAM4 is not as large as in CAM5 (Fig. 7). Interestingly, accompanied with an enhanced variability, the skewness values have also increased in the runs with observed wind climatology but keeping the model wind interannual anomalies (experiments 4a and 4b) relative to the runs with full model winds (experiments 3a and 3b). The results suggest that the improvement of mean winds will help to increase the simulation of ENSO asymmetry.

The effect of the bias in the mean winds on the tropical mean SST state also shows up in the runs with ENSO (Fig. 9). Compared to the effect in the runs without ENSO (Fig. 8), there is a much cooler warm pool in addition to an excessive cold tongue in the runs with ENSO. The distinct difference over the warm pool may manifest as the rectification effect of ENSO (Sun et al. 2014). A comparison of the SST differences in the bottom two rows of Fig. 9 (Figs. 9b,c,e,f) shows that the tropical Pacific SST tends toward a warming state when the model wind climatology is replaced with the observed counterpart. Linked to the difference in the skewness value (Table 1), the results indicate that a warmer mean SST state is in favor of the increase of ENSO asymmetry.

To better understand the skewness value listed in Table 1, Fig. 10 and Fig. 11 display the differences in composite SST anomalies of six sensitivity experiments from reference experiment 1 for the warm phase and the cold phase of ENSO, respectively. The magnitude of equatorial cold SST anomalies in the run forced by full CAM4 winds is much stronger than in the run by full CAM5 winds during the cold phase (Figs. 11b,e), while the difference in the SST warm anomalies between two runs forced by full model winds is relatively smaller (Figs. 10b,e). A quantitative measure of the Niño-3 SST anomaly difference reveals that the cold SST anomaly difference between these two runs is about 0.09°C, more than double the corresponding warm SST anomaly difference (about 0.04°C). This indicates that the difference in SST skewness between the two runs by full AMIP model winds mainly arises from the difference in negative SST anomalies during the cold phase of ENSO, which is also the dominant ENSO phase responsible for the difference in ENSO asymmetry from the two corresponding coupled models (Figs. 3 and 4).

We note that the SST warm anomalies are somewhat underestimated in the two runs by full model winds compared to those in the run by observed winds (Figs. 10b,e). This may result from the AMIP zonal wind stress bias that the westerly wind anomaly is positioned too far to the west along with a significant easterly wind anomaly in the far-eastern Pacific during the warm phase (Figs. 6a–c), similar to the problem noted in CMIP5 models (Zhang and Sun 2014). The comparison between experiment 3a and 3b and experiment 4a and 4b shows that a warmer SST mean state induced by observed mean winds can improve the simulation of ENSO asymmetry by increasing the magnitude of SST warm anomalies (Figs. 10b,c,e,f), as is particularly evident in the change from experiment 3b to experiment 4b due to the quite different wind climatology used.

4. Summary and discussion

To further explore the impacts of atmospheric processes on ENSO asymmetry, we have extended the

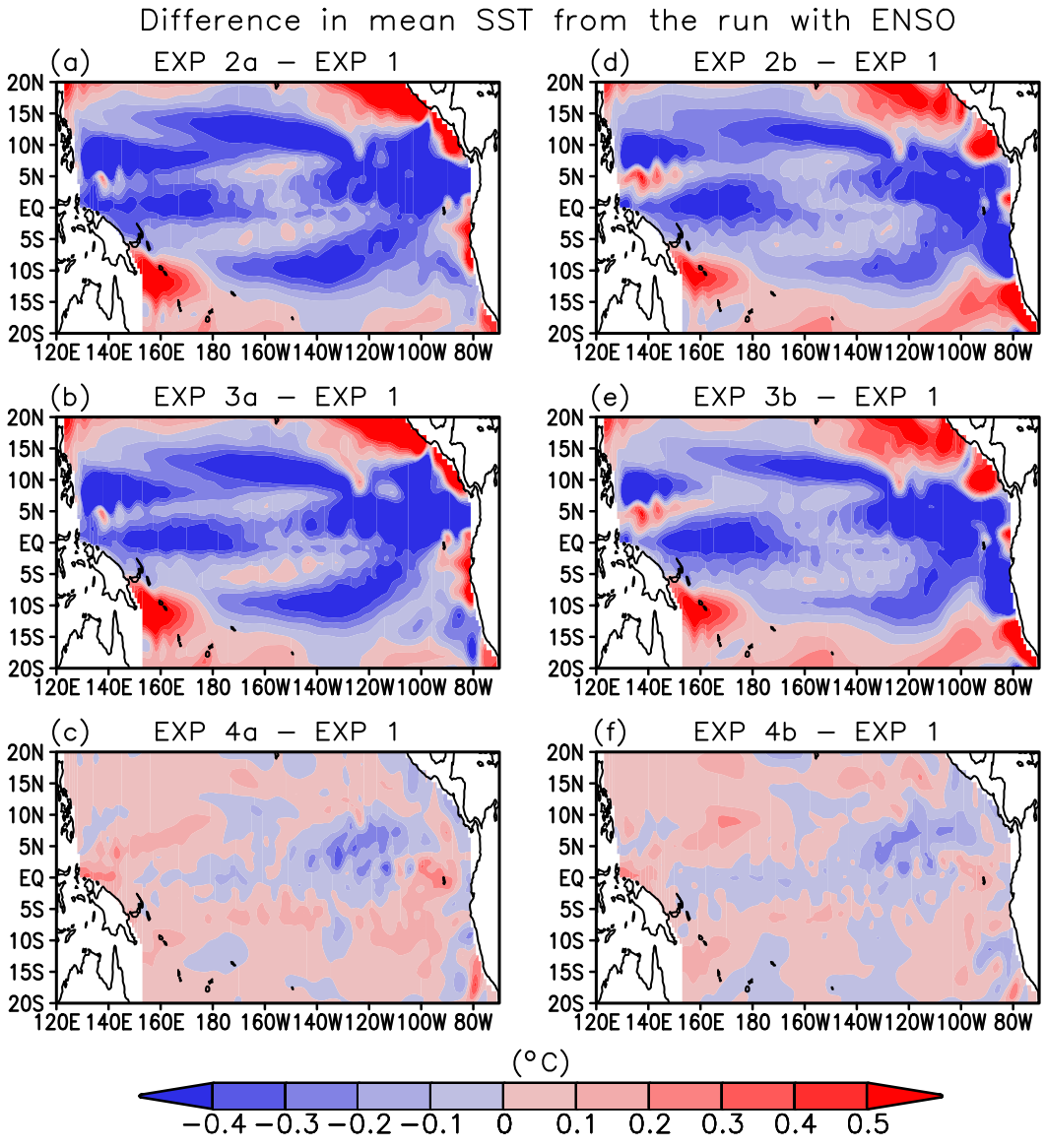

FIG. 9. Time-mean SST difference of (a)–(c) experiments 2a, 3a, and 4a and (d)–(f) experiments 2b, 3b, and 4b from experiment 1.

analysis of the ENSO asymmetry in CMIP5 models (Zhang and Sun 2014) to the latest two NCAR models—CESM1 and CCSM4. CESM1 has the same ocean component as CCSM4, with the biggest change occurring in the atmosphere component model. Therefore, our analysis will isolate the effects from atmospheric biases on ENSO asymmetry and help to identify the factors responsible for the improvement of ENSO modeling.

Our evaluation shows that in general an underestimate of the observed positive ENSO asymmetry measured by the skewness of Niño-3 SST anomalies remains a problem in the two latest NCAR coupled models. The weaker ENSO asymmetry is more prominent in CCSM4. By comparison, CESM1 is getting closer to the observations than CCSM4 in the simulation of ENSO asymmetry. The weaker ENSO asymmetry in the two models corresponds to a cold bias in the mean SST climatology as noted in many coupled models (Sun et al. 2006; Zhang et al. 2009; Zhang and Sun 2014; Sun et al. 2016). Interestingly, the cold bias in the mean SST state is more profound in CESM1 than in CCSM4, although the former shows an overall improvement in simulating the ENSO asymmetry. Different from most CMIP5 models in which the weaker SST anomaly associated with the warm phase of ENSO is the main

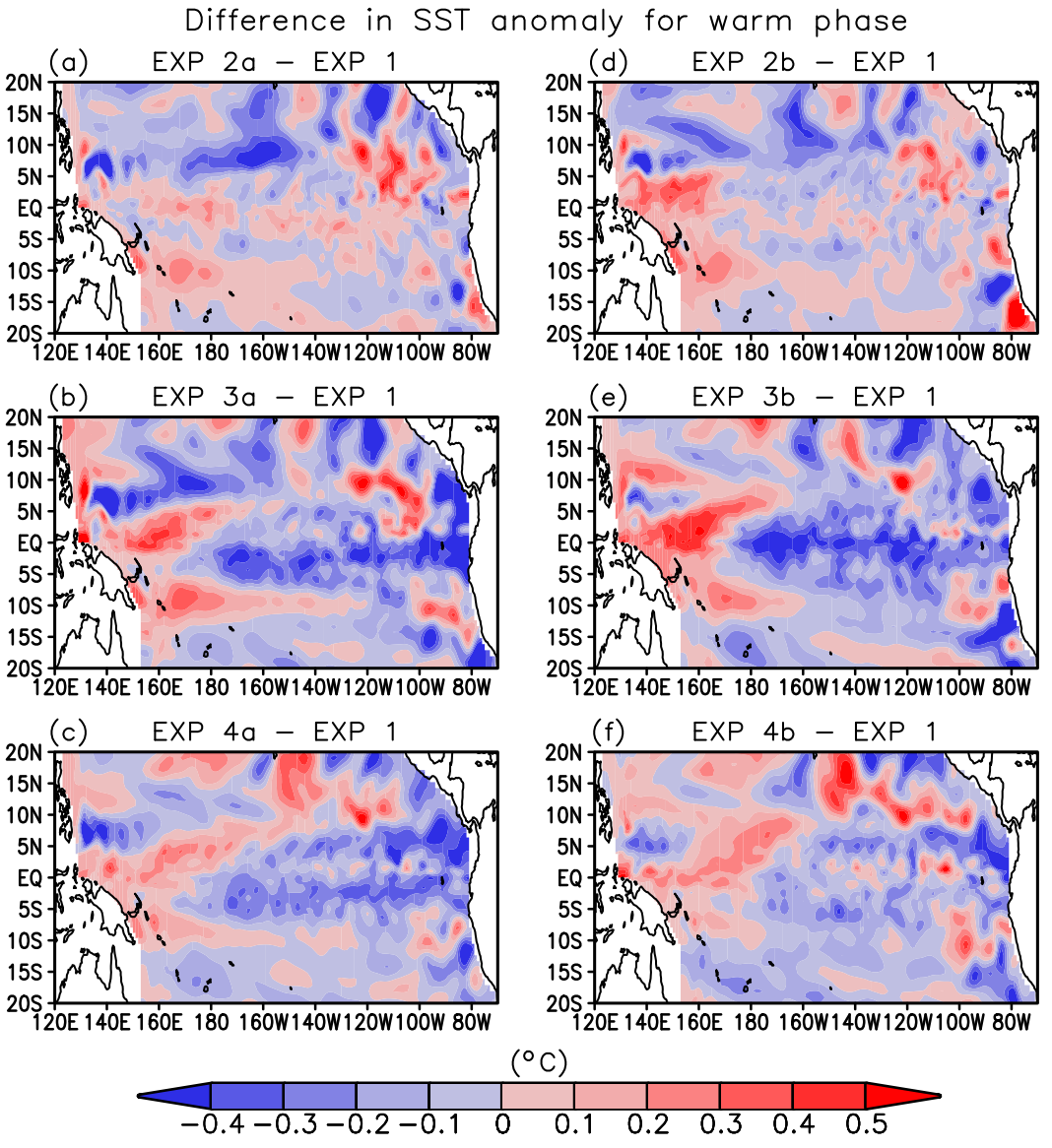

FIG. 10. As in Fig. 9, but for the difference in the SST anomaly during the warm phase.

contributor to the weak ENSO asymmetry (Zhang and Sun 2014; Sun et al. 2016), the two NCAR models simulate well the SST anomaly during the warm phase of ENSO. However, the negative SST anomaly during the cold phase of ENSO is too strong, especially in CCSM4, leading to the weak ENSO asymmetry in the models. The relatively larger ENSO asymmetry in CESM1 relative to CCSM4 also primarily results from the reduced bias in the negative SST anomaly during the cold phase of ENSO.

The analysis of the zonal wind stress and precipitation from the corresponding AMIP runs is further presented to understand whether the bias in the coupled models can be linked to the bias in the stand-alone atmosphere models. We have found that the two NCAR AMIP models have a weaker skewness of zonal wind stress than observations, even if the SST forcing has identical ENSO asymmetry as observed. Compared to CAM4, CAM5 has a broad increase in the simulation of zonal wind stress skewness across the equatorial Pacific, mainly due to a more westward shift of easterly wind anomaly along with a slight westward shift of the negative precipitation anomaly during the cold phase of ENSO. The discrepancy in the skewness of zonal wind stress in AMIP models may be responsible for the generally weaker ENSO asymmetry in the corresponding coupled models (CCSM4 and CESM1) and the improvement in simulating ENSO asymmetry in CESM1.

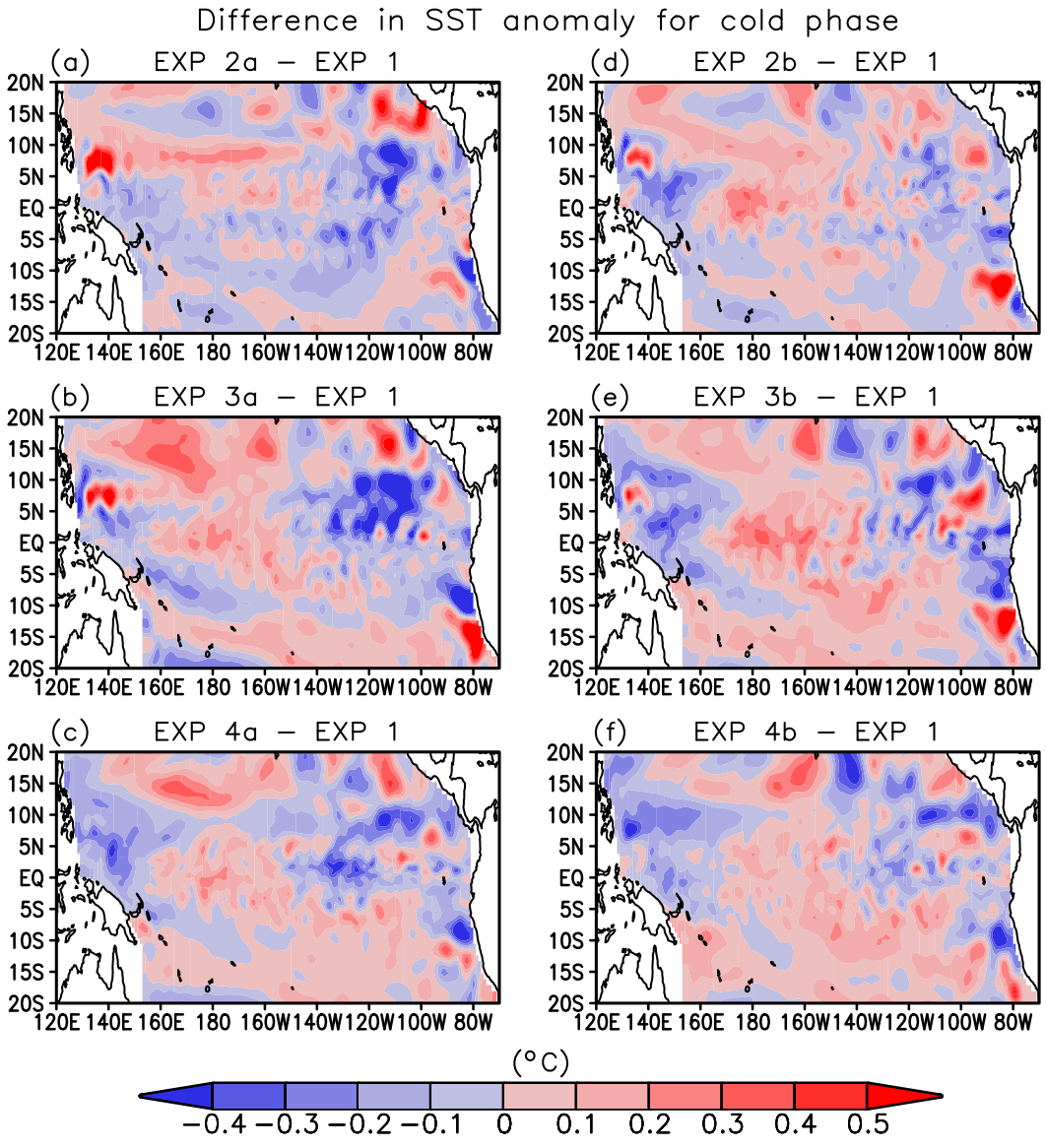

FIG. 11. As in Fig. 9, but for the difference in the SST anomaly during the cold phase.

We have also found that there is a stronger time mean equatorial zonal wind in the AMIP runs. By comparison, the bias of the stronger mean wind is more significant in CAM5 than in CAM4. The stronger mean winds in the former are accompanied with the changes in mean precipitation between the two AMIP models, featuring overall more (less) precipitation over the warm pool (cold tongue) region. The numerical experiment with a linear baroclinic model shows that the east–west asymmetry in the mean precipitation difference can drive the stronger mean winds in CAM5 model. This is because the excessive zonal latent heating gradient associated with zonal precipitation gradient may generate the stronger zonal pressure gradient force, which in turn produces the stronger mean winds (Lin 2007). The stronger tropical mean winds in CAM5 may contribute to the significant cold bias in SST mean state noted in CESM1 coupled runs. This argument is supported by the wind-forced ocean GCM experiments without ENSO, which indicate that the stronger climatological winds in CAM5 will trigger a stronger initial cold bias in mean SST. The stronger mean winds in CAM5 induced by changes in the mean precipitation distribution between the two AMIP models may be associated with the replacement of the Hack (1994) scheme used in CAM4 by the new shallow convection scheme (Park and Bretherton 2009) incorporated in CAM5. On the other hand, the change in shallow convection scheme from

CAM4 to CAM5 seems to improve the simulation of precipitation anomaly associated with ENSO, especially for the cold phase. The simulation of wind stress anomaly linked to the precipitation anomaly is therefore improved in CAM5, which has an increased skewness of interannual wind anomaly. A separate study is necessary to verify whether it is true that the update of shallow convection scheme deteriorates the simulation of tropical mean winds but improves the simulation of interannual wind anomaly, given the fact that there have been a number of other changes in parameterizations from CAM4 to CAM5 (see section 2).

The relative importance of biases in the mean and interannual variability of winds from the two AMIP runs to the simulation of ENSO asymmetry is explored based on wind-forced ocean model experiments with ENSO. The numerical experiments demonstrate that the bias in AMIP model winds can weaken ENSO asymmetry, with the contribution from the wind interannual variability being larger than from the mean winds. This implies that the weaker ENSO asymmetry in coupled models may originate from the bias in the stand-alone atmosphere model. We also note that the ENSO asymmetry in the run forced by CAM5 full winds is relatively greater than in the run by CAM4 full winds. Considering the relatively larger ENSO asymmetry in CESM1 than in CCSM4 and the same ocean component used in the two coupled models, our analysis pinpoints the pathway of improving ENSO asymmetry to the simulation of tropical Pacific winds in the stand-alone atmosphere model.

It has been suggested that there is a linkage between the ENSO asymmetry and tropical mean state (Sun et al. 2013, 2016). Zhang and Sun (2014) found that the warmer SST mean state will facilitate the increase of ENSO asymmetry by enhancing the SST warm anomalies, which is also confirmed in the present extended study. In addition to the effect of tropical mean winds and the resulting tropical SST mean state, the effect of wind interannual variability is also important to the simulation of ENSO asymmetry. We note that CAM5 has a stronger mean wind than CAM4 and the corresponding coupled CESM1 model has a larger cold bias in mean SST than CCSM4, but the ENSO asymmetry is still relatively larger in CAM5 wind-forced runs and CESM1 relative to CAM4 wind-forced runs and CCSM4. This improvement mainly results from the contribution of relatively larger skewness of interannual wind anomaly in CAM5. Therefore, our analysis suggests that the ENSO asymmetry may be inversely proportional to the magnitude of mean winds and proportional to the skewness of interannual wind anomaly. The strong ENSO activity, which is tied to the variance of Pacific winds, has also been found to be accompanied by the strong ENSO asymmetry in many coupled models (Sun et al. 2016). It should be noted that the present study only focuses on NCAR models. It is possible that the poor simulation of ENSO asymmetry in other models may have different reasons. Further studies are needed to explore a new metric for the representation of ENSO asymmetry in coupled models that reflects the effect of tropical Pacific wind characteristics.

Acknowledgments. This work was jointly supported by the National Natural Science Foundation of China (Fund 41528502), the Strategic Project of the Chinese Academy of Sciences (Grant XDA11010401), and NOAA's Climate Program Office.

REFERENCES

An, S.-I., and F.-F. Jin, 2004: Nonlinearity and asymmetry of ENSO. *J. Climate*, **17**, 2399–2412, https://doi.org/10.1175/1520-0442(2004)017<2399:NAAOE>2.0.CO;2.

——, Y.-G. Ham, J.-S. Kug, F.-F. Jin, and I.-S. Kang, 2005: El Niño–La Niña asymmetry in the Coupled Model Intercomparison Project simulations. *J. Climate*, **18**, 2617–2627, https://doi.org/10.1175/JCLI3433.1.

Bretherton, C. S., and S. Park, 2009: A new moist turbulence parameterization in the Community Atmosphere Model. *J. Climate*, **22**, 3422–3448, https://doi.org/10.1175/2008JCLI2556.1.

Burgers, G., and D. B. Stephenson, 1999: The ''normality'' of El Niño. *Geophys. Res. Lett.*, **26**, 1027–1030, https://doi.org/10.1029/1999GL900161.

Carton, J. A., and B. S. Giese, 2008: A reanalysis of ocean climate using Simple Ocean Data Assimilation (SODA). *Mon. Wea. Rev.*, **136**, 2999–3017, https://doi.org/10.1175/2007MWR1978.1.

Choi, J., S.-I. An, B. Dewitte, and W. W. Hsieh, 2009: Interactive feedback between the tropical Pacific decadal oscillation and ENSO in a coupled general circulation model. *J. Climate*, **22**, 6597–6611, https://doi.org/10.1175/2009JCLI2782.1.

Choi, K.-Y., G. A. Vecchi, and A. T. Wittenberg, 2013: ENSO transition, duration, and amplitude asymmetries: Role of the nonlinear wind stress coupling in a conceptual model. *J. Climate*, **26**, 9462–9476, https://doi.org/10.1175/JCLI-D-13-00045.1.

Collins, W. D., 2001: Parameterization of generalized cloud overlap for radiative calculations in general circulation models *J. Atmos. Sci.*, **58**, 3224–3242, https://doi.org/10.1175/1520-0469(2001)058<3224:POGCOF>2.0.CO;2.

——, J. K. Hackney, and D. P. Edwards, 2002: An updated parameterization for infrared emission and absorption by water vapor in the National Center for Atmospheric Research Community Atmosphere Model. *J. Geophys. Res.*, **107**, 4664, https://doi.org/10.1029/2001JD001365.

Frauen, C., and D. Dommenget, 2010: El Niño and La Niña amplitude asymmetry caused by atmospheric feedbacks. *Geophys. Res. Lett.*, **37**, L18801, https://doi.org/10.1029/2010GL044444.

Gent, P. R., and M. A. Cane, 1989: A reduced gravity, primitive equation model of the upper equatorial ocean. *J. Comput. Phys.*, **81**, 444–480, https://doi.org/10.1016/0021-9991(89)90216-7.

——, and Coauthors, 2011: The Community Climate System Model version 4. *J. Climate*, **24**, 4973–4991, https://doi.org/10.1175/2011JCLI4083.1.

Hack, J. J., 1994: Parameterization of moist convection in the National Center for Atmospheric Research Community Climate Model (CCM2). *J. Geophys. Res.*, **99**, 5551–5568, https://doi.org/10.1029/93JD03478.

Hannachi, A., D. Stephenson, and K. Sperber, 2003: Probability-based methods for quantifying nonlinearity in the ENSO. *Climate Dyn.*, **20**, 241–256, https://doi.org/10.1007/s00382-002-0263-7.

Hoell, A., M. Hoerling, J. Eischeid, K. Wolter, R. Dole, J. Perlwitz, T. Xu, and L. Cheng, 2016: Does El Niño intensity matter for California precipitation? *Geophys. Res. Lett.*, **43**, 819–825, https://doi.org/10.1002/2015GL067102.

Hoerling, M. P., A. Kumar, and M. Zhong, 1997: El Niño, La Niña, and the nonlinearity of their teleconnections. *J. Climate*, **10**, 1769–1786, https://doi.org/10.1175/1520-0442(1997)010<1769:ENOLNA>2.0.CO;2.

Holtslag, A. A. M., and B. A. Boville, 1993: Local versus nonlocal boundary-layer diffusion in a global climate model. *J. Climate*, **6**, 1825–1842, https://doi.org/10.1175/1520-0442(1993)006<1825:LVNBLD>2.0.CO;2.

Hurrell, J. W., and Coauthors, 2013: The Community Earth System Model: A framework for collaborative research. *Bull. Amer. Meteor. Soc.*, **94**, 1339–1360, https://doi.org/10.1175/BAMS-D-12-00121.1.

Iacono, M. J., J. S. Delamere, E. J. Mlawer, M. W. Shephard, S. A. Clough, and W. D. Collins, 2008: Radiative forcing by long-lived greenhouse gases: Calculations with the AER radiative transfer models. *J. Geophys. Res.*, **113**, D13103, https://doi.org/10.1029/2008JD009944.

Im, S.-H., S.-I. An, S. T. Kim, and F.-F. Jin, 2015: Feedback processes responsible for El Niño–La Niña amplitude asymmetry. *Geophys. Res. Lett.*, **42**, 5556–5563, https://doi.org/10.1002/2015GL064853.

Jin, F.-F., S.-I. An, A. Timmermann, and J. Zhao, 2003: Strong El Niño events and nonlinear dynamical heating. *Geophys. Res. Lett.*, **30**, 1120, https://doi.org/10.1029/2002GL016356.

Kang, I.-S., and J.-S. Kug, 2002: El Niño and La Niña sea surface temperature anomalies: Asymmetry characteristics associated with their wind stress anomalies. *J. Geophys. Res.*, **107**, 4372, https://doi.org/10.1029/2001JD000393.

Kiladis, G. N., and H. Diaz, 1989: Global climatic anomalies associated with extremes in the Southern Oscillation. *J. Climate*, **2**, 1069–1090, https://doi.org/10.1175/1520-0442(1989)002<1069:GCAAWE>2.0.CO;2.

Larkin, N. K., and D. E. Harrison, 2005: On the definition of El Niño and associated seasonal average U.S. weather anomalies. *Geophys. Res. Lett.*, **32**, L13705, https://doi.org/10.1029/2005GL022738.

Lin, J.-L., 2007: The double-ITCZ problem in IPCC AR4 coupled GCMs: Ocean–atmosphere feedback analysis. *J. Climate*, **20**, 4497–4525, https://doi.org/10.1175/JCLI4272.1.

Liu, X., and Coauthors, 2012: Toward a minimal representation of aerosols in climate models: Description and evaluation in the Community Atmosphere Model CAM5. *Geosci. Model Dev.*, **5**, 709–739, https://doi.org/10.5194/gmd-5-709-2012.

Meehl, G. A., and Coauthors, 2013: Climate change projections in CESM1(CAM5) compared to CCSM4. *J. Climate*, **26**, 6287–6308, https://doi.org/10.1175/JCLI-D-12-00572.1.

Morrison, H., and A. Gettelman, 2008: A new two-moment bulk stratiform cloud microphysics scheme in the Community Atmosphere Model (CAM3), version 3. Part I: Description and numerical tests. *J. Climate*, **21**, 3642–3659, https://doi.org/10.1175/2008JCLI2105.1.

Neale, R. B., J. H. Richter, and M. Jochum, 2008: The impact of convection on ENSO: From a delayed oscillator to a series of events. *J. Climate*, **21**, 5904–5924, https://doi.org/10.1175/2008JCLI2244.1.

——, and Coauthors, 2012: Description of the NCAR Community Atmosphere Model (CAM 5.0). NCAR Tech. Note NCAR/TN-486+STR, 274 pp., http://www.cesm.ucar.edu/models/cesm1.0/cam/docs/description/cam5_desc.pdf.

——, J. Richter, S. Park, P. H. Lauritzen, S. J. Vavrus, P. J. Rasch, and M. Zhang, 2013: The mean climate of the Community Atmosphere Model (CAM4) in forced SST and fully coupled experiments. *J. Climate*, **26**, 5150–5168, https://doi.org/10.1175/JCLI-D-12-00236.1.

Park, S., and C. S. Bretherton, 2009: The University of Washington shallow convection and moist turbulence schemes and their impact on climate simulations with the Community Atmosphere Model. *J. Climate*, **22**, 3449–3469, https://doi.org/10.1175/2008JCLI2557.1.

Peng, S., and J. S. Whitaker, 1999: Mechanisms determining the atmospheric response to midlatitude SST anomalies. *J. Climate*, **12**, 1393–1408, https://doi.org/10.1175/1520-0442(1999)012<1393:MDTART>2.0.CO;2.

Philip, S., and G. J. van Oldenborgh, 2009: Significant atmospheric nonlinearities in the ENSO cycle. *J. Climate*, **22**, 4014–4028, https://doi.org/10.1175/2009JCLI2716.1.

Rasch, P. J., and J. E. Kristjánsson, 1998: A comparison of the CCM3 model climate using diagnosed and predicted condensate parameterizations. *J. Climate*, **11**, 1587–1614, https://doi.org/10.1175/1520-0442(1998)011<1587:ACOTCM>2.0.CO;2.

Rayner, N. A., D. E. Parker, E. B. Horton, C. K. Folland, L. V. Alexander, D. P. Rowell, E. C. Kent, and A. Kaplan, 2003: Global analyses of sea surface temperature, sea ice, and night marine air temperature since the late nineteenth century. *J. Geophys. Res.*, **108**, 4407, https://doi.org/10.1029/2002JD002670.

Rodgers, K. B., P. Friederichs, and M. Latif, 2004: Tropical Pacific decadal variability and its relation to decadal modulation of ENSO. *J. Climate*, **17**, 3761–3774, https://doi.org/10.1175/1520-0442(2004)017<3761:TPDVAI>2.0.CO;2.

Ropelewski, C. F., and M. S. Halpert, 1987: Global and regional scale precipitation patterns associated with the El Niño/Southern Oscillation. *Mon. Wea. Rev.*, **115**, 1606–1626, https://doi.org/10.1175/1520-0493(1987)115<1606:GARSPP>2.0.CO;2.

Schopf, P. S., and R. J. Burgman, 2006: A simple mechanism for ENSO residuals and asymmetry. *J. Climate*, **19**, 3167–3179, https://doi.org/10.1175/JCLI3765.1.

Smith, R. D., and Coauthors, 2010: The Parallel Ocean Program (POP) reference manual: Ocean component of the Community Climate System Model (CCSM) and Community Earth System Model (CESM). Los Alamos National Laboratory Tech. Rep. LAUR-10-01853, 141 pp., www.cesm.ucar.edu/models/cesm1.0/pop2/doc/sci/POPRefManual.pdf.

Su, J., R. Zhang, T. Li, X. Rong, J.-S. Kug, and C.-C. Hong, 2010: Causes of the El Niño and La Niña amplitude asymmetry in the equatorial eastern Pacific. *J. Climate*, **23**, 605–617, https://doi.org/10.1175/2009JCLI2894.1.

Sun, D.-Z., 2003: A possible effect of an increase in the warm-pool SST on the magnitude of El Niño warming. *J. Climate*, **16**, 185–205, https://doi.org/10.1175/1520-0442(2003)016<0185:APEOAI>2.0.CO;2.

——, and T. Zhang, 2006: A regulatory effect of ENSO on the time-mean thermal stratification of the equatorial upper ocean. *Geophys. Res. Lett.*, **33**, L07710, https://doi.org/10.1029/2005GL025296.

——, ——, and S.-I. Shin, 2004: The effect of subtropical cooling on the amplitude of ENSO: A numerical study. *J. Climate*, **17**,

3786–3798, https://doi.org/10.1175/1520-0442(2004)017<3786:TEOSCO>2.0.CO;2.

——, and Coauthors, 2006: Radiative and dynamical feedbacks over the equatorial cold tongue: Results from nine atmospheric GCMs. *J. Climate*, **19**, 4059–4074, https://doi.org/10.1175/JCLI3835.1.

——, T. Zhang, Y. Sun, and Y. Yu, 2014: Rectification of El Niño–Southern Oscillation into climate anomalies of decadal and longer time scales: Results from forced ocean GCM experiments. *J. Climate*, **27**, 2545–2561, https://doi.org/10.1175/JCLI-D-13-00390.1.

Sun, F., and J.-Y. Yu, 2009: A 10–15-yr modulation cycle of ENSO intensity. *J. Climate*, **22**, 1718–1735, https://doi.org/10.1175/2008JCLI2285.1.

Sun, Y., D.-Z. Sun, L. X. Wu, and F. Wang, 2013: Western Pacific warm pool and ENSO asymmetry in CMIP3 models. *Adv. Atmos. Sci.*, **30**, 940–953, https://doi.org/10.1007/s00376-012-2161-1.

——, F. Wang, and D.-Z. Sun, 2016: Weak ENSO asymmetry due to weak nonlinear air–sea interaction in CMIP5 climate models. *Adv. Atmos. Sci.*, **33**, 352–364, https://doi.org/10.1007/s00376-015-5018-6.

Taschetto, A. S., A. Sen Gupta, N. C. Jourdain, A. Santoso, C. C. Ummenhofer, and M. H. England, 2014: Cold tongue and warm pool ENSO events in CMIP5: Mean state and future projections. *J. Climate*, **27**, 2861–2885, https://doi.org/10.1175/JCLI-D-13-00437.1.

Taylor, K. E., R. J. Stouffer, and G. A. Meehl, 2012: An overview of CMIP5 and the experiment design. *Bull. Amer. Meteor. Soc.*, **93**, 485–498, https://doi.org/10.1175/BAMS-D-11-00094.1.

van Oldenborgh, G. J., S. Philip, and M. Collins, 2005: El Niño in a changing climate: A multi-model study. *Ocean Sci.*, **1**, 81–95, https://doi.org/10.5194/os-1-81-2005.

Vialard, J., C. Menkes, J.-P. Boulanger, P. Delecluse, E. Guilyardi, M. J. McPhaden, and G. Madec, 2001: A model study of oceanic mechanisms affecting equatorial Pacific sea surface temperature during the 1997–98 El Niño. *J. Phys. Oceanogr.*, **31**, 1649–1675, https://doi.org/10.1175/1520-0485(2001)031<1649:AMSOOM>2.0.CO;2.

Wallace, J. M., E. M. Rasmusson, T. P. Mitchell, V. E. Kousky, E. S. Sarachik, and H. von Storch, 1998: On the structure and evolution of ENSO-related climate variability in the tropical Pacific: Lessons from TOGA. *J. Geophys. Res.*, **103**, 14 241–14 259, https://doi.org/10.1029/97JC02905.

Xie, P., and P. A. Arkin, 1997: Global precipitation: A 17-year monthly analysis based on gauge observations, satellite estimates, and numerical model outputs. *Bull. Amer. Meteor. Soc.*, **78**, 2539–2558, https://doi.org/10.1175/1520-0477(1997)078<2539:GPAYMA>2.0.CO;2.

Yeh, S.-W., and B. Kirtman, 2004: Tropical Pacific decadal variability and ENSO amplitude modulation in a CGCM. *J. Geophys. Res.*, **109**, C11009, https://doi.org/10.1029/2004JC002442.

Zhang, T., and D.-Z. Sun, 2014: ENSO asymmetry in CMIP5 models. *J. Climate*, **27**, 4070–4093, https://doi.org/10.1175/JCLI-D-13-00454.1.

——, ——, R. Neale, and P. J. Rasch, 2009: An evaluation of ENSO asymmetry in the Community Climate System Models: A view from the subsurface. *J. Climate*, **22**, 5933–5961, https://doi.org/10.1175/2009JCLI2933.1.

——, M. P. Hoerling, J. Perlwitz, D.-Z. Sun, and D. Murray, 2011: Physics of U.S. surface temperature response to ENSO. *J. Climate*, **24**, 4874–4887, https://doi.org/10.1175/2011JCLI3944.1.

——, J. Perlwitz, and M. P. Hoerling, 2014: What is responsible for the strong observed asymmetry in teleconnections between El Niño and La Niña? *Geophys. Res. Lett.*, **41**, 1019–1025, https://doi.org/10.1002/2013GL058964.

——, M. P. Hoerling, J. Perlwitz, and T. Xu, 2016: Forced atmospheric teleconnections during 1979–2014. *J. Climate*, **29**, 2333–2357, https://doi.org/10.1175/JCLI-D-15-0226.1.